Surface & Coatings Technology 354 (2018) 92–100

Contents lists available at ScienceDirect

Surface & Coatings Technology

journal homepage: www.elsevier.com/locate/surfcoat

Microstructure and tribological behavior of plasma sprayed NiCrAlY/WC-Co/cenosphere/solid lubricants composite coatings

Mrityunjay Doddamani[a], Mahantayya Mathapati[b,*], M.R. Ramesh[b]

[a] Department of Mechanical Engineering, National Institute of Technology Karnataka, Surathkal, India
[b] Department of Mechanical Engineering, KLE College of Engineering and Technology, Chikodi, karnataka, India

ARTICLE INFO

Keywords:
Plasma spray
Cenospheres
Solid lubricants
Wear
NiCrAlY

ABSTRACT

Present investigation deal with NiCrAlY/WC-Co/Cenosphere/MoS_2/CaF_2, NiCrAlY/WC-Co/Cenosphere/MoS_2/$CaSO_4$ and NiCrAlY/WC-Co/Cenosphere coatings deposited on MDN 321 steel using atmospheric plasma spraying. Tribological properties of MDN 321 steel and coatings are evaluated from room temperature (RT) to 600 °C under dry lubrication conditions using a pin on disc high-temperature tribometer. Scanning Electron Microscopy (SEM), X-ray diffraction (XRD) and Energy Dispersive Spectroscopy (EDS) are used to characterize the coatings. Presence of cenospheres in these coatings might effectively reduce wear acting as localized regions accumulating wear debris. The result shows that wear rate of all the coatings are lower as compared to MDN 321 substrate at all the test conditions. NiCrAlY/WC-Co/Cenosphere/MoS_2/CaF_2 and NiCrAlY/WC-Co/Cenosphere/MoS/$CaSO_4$ coatings registered lower friction coefficient as compared to NiCrAlY/WC-Co/Cenosphere coating and MDN 321 substrate. Characterization of the NiCrAlY/WC-Co/Cenosphere/MoS_2/CaF_2 and NiCrAlY/WC-Co/Cenosphere/MoS_2/$CaSO_4$ coatings worn out surface suggests that MoS_2 provides lubrication at 200 °C and formation of $CaMoO_4$, MoO_3 through tribo chemistry reaction at higher temperature provides lubrication at 600 °C. SEM micrograph of worn surface demonstrates that the main wear mechanism is plowing and delamination.

1. Introduction

Components working at higher operating temperatures like in gas and steam turbines, propulsion bearings, air foil bearings and internal combustion engines are subjected to surface friction and wear [1–4]. Solid lubricant coatings are effective in minimizing friction and wear under harsh environments like high temperature, vacuum and high humidity where conventional lubricants such as oil and grease fail to sustain their integrity [5–7]. Commonly available solid lubricants are transition metal disulfides (MoS_2, WS_2, TaS_2), soft noble metals (Au, Ag), inorganic fluorides (CaF_2, BaF_2, etc.) and metal oxides (NiO, Cr_2O_3, etc.) [8,9]. However, the sole lubricant may not provide the lubrication over a wide range of operating temperatures. For example, MoS_2 loses its lubricity above 300 °C owing to oxidation and cannot be used for high-temperature applications. CaF_2 and BaF_2 are effective at elevated temperature (> 500 °C) due to their low shear strength at higher temperature [10]. Many researches have incorporated these low and high-temperature solid lubricants in the coatings to achieve the synergetic effect over wide temperature range [8,11–13].

Plasma sprayed NiCrAlY coatings are widely used in the higher temperature applications to combat the effects of oxidation, corrosion and wear resistance. However, these coatings find limitations in industries due to lower hardness as compared to carbides, ceramics, and oxides [14–16]. Nevertheless, wear resistance of these coatings can be significantly improved by reinforcing the hard phases like WC, Al_2O_3, Cr_3C_2, Cr_2O_3, ZrO_2 etc. [17]. WC-Co possesses higher hardness, better ductility, chemical inertness and lower frictional values as compared to Cr_3C_2 [18]. These properties of WC-Co improve the wear resistance of NiCrAlY coating when reinforced as a hard phase. Further, WC-Co coatings possess high frictional values at higher temperature necessitating the incorporation of solid lubricants in the coating. Chen et al. [1] studied the friction and wear behavior of plasma sprayed NiCrAlY-Ag-Mo coating at different temperatures and reported that, the addition of Ag and Mo decreased the friction coefficient and wear rate. Joel and Basil [19] investigated the WC-10Ni/MoS_2/WS_2 coating by HVOF and they found 50% reduction in mass loss of the coating as compared to WC-10Ni. Bin C et al. [20] studied the tribological behavior of graphite/CaF_2/TiC/Ni-base alloy coating by plasma spray and reported that friction coefficient and wear rate are reduced by 25.9–53% and 18.6–70.1% compared to Ni base alloy coating respectively. However,

* Corresponding author.
E-mail address: mahantkm@gmail.com (M. Mathapati).

https://doi.org/10.1016/j.surfcoat.2018.09.018
Received 27 February 2018; Received in revised form 5 September 2018; Accepted 7 September 2018
Available online 08 September 2018

NiCrAlY and WC-Co powders are the quite expensive demanding development of low cost cenosphere coatings. Incorporation of the inexpensive hollow cenospheres in the coatings might effectively reduce the wear by opening up the built-in porosity which can act as localized regions for wear debris accumulation. Elemental constituents of cenospheres can reduce wear further.

Fly ash cenospheres are industrial waste from thermal power plants, generated due to combustion of coal. These fly ash cenospheres are spherical in shape, readily available in powder form, inexpensive and possess superior mechanical properties [21–26]. The main constituents of fly ash cenospheres are oxides of silicon (SiO_2), aluminium (Al_2O_3), iron (Fe_2O_3) and mullite ($3Al_2O_3{\cdot}2SiO_2$) [27–31]. Among them, aluminium oxide and mullite possess high-temperature stability, wear, erosion, and corrosion resistance [32,33]. These properties can be well exploited by incorporating fly ash cenospheres in the coatings. Some researchers have developed the coatings using fly ash and their study reveals that fly ash can be effectively used as feedstock for plasma spray coatings [34,35]. Rama Krishna et al. [36] investigated the wear response of detonation sprayed fly ash coating on mild steel. They found that fly ash coating has a lower coefficient of friction compared to mild steel. Sidhu et al. [37] studied the wear, oxidation and salt corrosion behavior of fly ash coating deposited using plasma spray. They reported better oxidation and salt corrosion resistance of fly ash coating as compared to carbon steel substrate. Behera and Mishra [38] investigated the fly ash composite coating deposited on the copper substrate by using plasma spray technique and results reveal better interfacial adhesion between substrate and coating. Available literature is relatively scarce on the usage of fly ash composite coatings using solid lubricants for high temperature wear resistance applications. This fact necessitates the study of elevated temperature wear behavior of composite coatings containing cenospheres and solid lubricants. Furthermore, understanding the wear mechanism of metallic matrix coatings with hollow cenospheres is an interesting and worth investigating task. Usage of such environmental pollutants in coatings might further reduce landfill burden and if developed successfully are eco-friendly as well.

In the present work, NiCrAlY-WC-Co/Cenosphere/MoS_2/CaF_2 (designated as $NiCaF_2$), NiCrAlY-WC-Co/Cenosphere/MoS_2/$CaSO_4$ (designated as $NiCaSO_4$) and NiCrAlY-WC-Co/Cenosphere (designated as Ni-WC) coatings are deposited on MDN 321 steel using plasma spray process. Sliding wear behavior of MDN 321 steel and coatings are evaluated at room temperature (RT), 200, 400 and 600 °C using a pin on disc high-temperature tribometer. The worn surfaces are analyzed and discussed in detail.

2. Materials and methods

2.1. Materials

MDN 321 steel is used as a substrate which is procured from Mishra Dhatu Nigam Ltd., Hyderabad, India, having chemical composition is Fe-0.1C-1.46Mn-18.13Cr-10.36Ni-0.62Ti-0.55Si (wt%). The substrate is trimmed to the dimension of 12 × 12 × 4 mm using a diamond saw prior to plasma spraying. Commercially available gas atomized NiCrAlY, agglomerated and sintered WC-Co (Powder Alloy Corporation, USA), fly ash cenospheres (Cenospheres India Pvt. Ltd., Kolkata, India) and laboratory reagent grade MoS_2, CaF_2 and $CaSO_4$ (Loba Chemie Pvt. Ltd., Mumbai, India) solid lubricants are utilized to prepare coating feedstock. Laser diffraction technique (Cilas, 1064, France) is used to measure the nominal size distribution of the powders and is reported in Table 1. These powders are blended mechanically with predetermined mass fraction before getting sprayed. Compositions of the coatings are listed in Table 2. Fig. 1a and b shows the SEM (JSM 6380LA, JEOL, JAPAN) micrographs of the blended $NiCaF_2$ and $NiCaSO_4$ mix respectively. It is observed from the micrographs that all the powders are mixed uniformly. NiCrAlY, WC-Co, and cenospheres are in spherical shape as shown in Fig. 1 and MoS_2, CaF_2 and $CaSO_4$ are irregular in shape.

Table 1
Particle size (μm) distribution of powders.

Particle size	NiCrAlY	WC-Co	Cenospheres[a]	MoS_2	CaF_2	$CaSO_4$
D (0.1)	41.88	23.52	–	0.63	4.27	8.72
D (0.5)	70.75	38.78	–	5.95	57.52	63.79
D (0.9)	120.33	64.11	–	29.45	115.52	132.57
0–10%	–	–	106	–	–	–
70–90%	–	–	63	–	–	–
0–30%	–	–	53	–	–	–
Mean	76.54	41.71	65	10.62	60.30	70.00

[a] As specified by Cenosphere India Pvt. Ltd., Kolkata, India.

Table 2
Composition of coatings (wt%).

Coatings	NiCrAlY	WC/Co	Cenospheres	MoS_2	CaF_2	$CaSO_4$
$NiCaF_2$	37.5	12.5	30	10	10	–
$NiCaSO_4$	37.5	12.5	30	10	–	10
Ni-WC	52.5	17.5	30	–	–	–

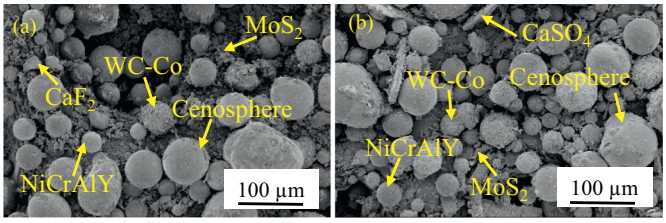

Fig. 1. Morphology of as blended (a) $NiCaF_2$ and (b) $NiCaSO_4$ powders.

2.2. Coating deposition and characterization

Atmospheric plasma spray technique is used to deposit $NiCaF_2$ and $NiCaSO_4$ blend using METCO USA 3 MB equipment (M/s. Spraymet Surface Technologies Pvt. Ltd., Bangalore, India). Substrates are grit blasted using alumina powder of 150 μm size before spraying to ensure better adhesion between the coating and substrate. NiCr bond coat is applied on the substrate prior to the spraying of $NiCaF_2$ and $NiCaSO_4$ coatings. Details of spray parameters are listed in Table 3. During spraying blended powder is loaded into the hopper which flows through the feeder and gets mixed with argon gas flowing from the compressor at a predefined pressure. This mixture flows towards the plasma stream and gets deposited on to the substrate. Deposition efficiency of coatings is about 40–45% and deposition per pass is in the range of 12–15 μm. SEM is used to measure the thickness of the developed coatings. Porosity of coatings is computed using optical microscope supported with biovis image analyzer (ARTRAY, AT 130, JAPAN). Twenty field of views are analyzed and average values are reported. XRD (DX GE-2P, JEOL, Japan) is employed to analyse the phases in blended powder and

Table 3
Plasma spray process parameters [41].[a]

Argon	Pressure	0.75 MPa
	Flow	40 lpm
Hydrogen	Pressure	0.35 MPa
	Flow	7 lpm
Current		490 A
Voltage		60 V
Powder feed rate		60 g/min
Stand of distance		100–125 mm

[a] As provided by Spraymet Surface Technology Pvt. Ltd., Bangalore, India.

coatings.

2.3. Microhardness and adhesion strength

Microhardness of the coatings and substrate is measured using OMNITECH Vickers microhardness tester on the polished cross section of the sample with a normal load of 300 g. Average values are reported from 20 indentations taken at different locations. The adhesion strength of the coatings is obtained using the pull-off method as outlined in ASTM C-633-13. Universal Testing Machine (Shimadzu hydraulic tensile machine, AG-X Plus, JAPAN) is utilized to carry out the test in tension mode with strain rate of 0.016 mm/s. The cylindrical samples of dimension Ø25 × 25 mm are used for the adhesion strength test. HTK Ultra bond epoxy resin is used as an adhesive to glue the coated samples with the counter blocks. Further, these samples are cured in the tubular furnace (Heatron Industrial Heaters, INDIA) at 150 °C for 3 h. The adhesion strength is computed by taking the ratio of maximum load to cross sectional area and the average values of five replicates are reported.

2.4. Sliding wear test

Sliding wear test is carried out using high temperature pin on disc tribometer (TR-20LE-PHM 400-CHM 600, Ducom Instruments Pvt. Ltd., Bangalore, India) under dry conditions as per ASTM G99-05. Alumina disc is used as the counter body. Sliding wear tests are conducted under a normal load of 20 and 40 N at sliding velocity of 1.5 m/s with a constant sliding distance of 3000 m. The test temperatures chosen are RT, 200, 400 and 600 °C. A computer-aided data acquisition system is utilized to concurrently record both height loss (using in built displacement transducer) and frictional force. Wear rate is calculated by converting the height loss into volume loss using the pin cross section area and expressed in terms of mm^3/m [21]. Subsequent to wear test, the worn surfaces and wear debris are observed through SEM. The elemental composition of wear debris is determined using EDS (JSM 6380LA, JEOL, JAPAN).

3. Results and discussion

3.1. Microstructure analysis of coating

SEM micrographs of polished cross section of $NiCaF_2$, $NiCaSO_4$ coatings and cross sectional EDS analysis of $NiCaF_2$ coating is shown in Fig. 2. The NiCr bond coat is well adhered with the substrate as well as coating thereby increases the adhesive strength between the substrate and coating. The average thickness of bond coat and coatings are 100 and 400 μm for both the coatings respectively. Porosity of $NiCaF_2$ and $NiCaSO_4$ coatings noted to be 4.1 ± 0.3 and 4.0 ± 0.3% respectively. The circled area in Fig. 2a and c is enlarged and presented in Fig. 2b and d respectively. From Fig. 2b and d, it is observed that coating constituents are distributed uniformly with fully melted splats and some semi melted particles, which are bonded together. Coatings mainly consist of cenosphere phase (dark gray), NiCrAlY phase (light gray) and WC-Co phase (white color) along with MoS_2, CaF_2, and $CaSO_4$ phases. Fig. 2e depicts the cross sectional elemental mapping of $NiCaF_2$ coating affirming uniform distribution of all the coating constituents. Fig. 2f displays the elemental overlay of the coating in weight percentage.

3.2. XRD analysis

The X-ray diffraction pattern of $NiCaF_2$ and $NiCaSO_4$ blended powder and as sprayed coatings are presented in Fig. 3a and b respectively. The result depicts that blended powder of $NiCaF_2$ (Fig. 3a) mainly consist of Ni, SiO_2, Al_2O_3 phases along with minor phases of $3Al_2O_32SiO_2$, WC, MoS_2, and CaF_2. XRD pattern of as deposited $NiCaF_2$ coating consists of Al_2O_3 and $AlNi_3$ as a major phases and MoS_2, CaF_2 and W_2C as a minor phases. W_2C is detected in the as deposited coating owing to the decarburization of WC during plasma spraying. WC decomposes significantly into W_2C during spraying owing to higher temperatures in the plasma spray process. Similar phases are observed in the XRD pattern of $NiCaSO_4$ blended powder and as sprayed coating as seen in $NiCaF_2$ except CaF_2, which is replaced by $CaSO_4$ (Fig. 3b).

Fig. 4a displays the XRD patterns of worn surfaces of $NiCaF_2$ coating after 200, 400 and 600 °C wear tests. Peaks of MoS_2 appear on worn surfaces at 200 °C as seen from Fig. 4a. On the contrary at 400 and 600 °C test temperatures, the intensity of peaks are reduced indicating MoS_2 is active at 200 °C. Smaller peaks of CaF_2 are noticed at 400 °C. Further, these peaks become strong at 600 °C implying lubrication at higher temperatures by CaF_2. New phases of $CaMoO_4$ and MoO_3 are observed at 600 °C suggesting molybdenum's reaction with calcium and oxygen forming molybdates and molybdenum oxide, which are responsible for lower coefficient of friction and wear rate at higher temperatures [1,39,40].

Fig. 4b demonstrates the XRD pattern of worn surfaces of $NiCaSO_4$ coating at 200, 400 and 600 °C wear tests. At 200 °C, $CaSO_4$ and distinct peaks of MoS_2 are observed indicating the formation of MoS_2 on the surface during wear test. At 400 °C, it is noticed that intensity of $CaSO_4$ peak is increased and some peaks of MoS_2 are disappeared implying dominancy of $CaSO_4$ at 400 °C. At 600 °C distinct peaks of $CaMoO_4$ and MoO_3 are observed as a result of the oxidation.

3.3. Microhardness and adhesion strength

The average microhardness of the substrate, $NiCaF_2$, and $NiCaSO_4$ coatings is 190 ± 10, 352 ± 30 and 370 ± 25 HV respectively. The microhardness of $NiCaF_2$ and $NiCaSO_4$ coatings diminished compared to NiCrAlY/WC-Co/cenosphere coating [41] owing to the addition of soft solid lubricants MoS_2, CaF_2, and $CaSO_4$. These low hardness solid lubricants are expected to impart low friction in dry sliding wear test [42].

Fig. 5a and b represent fractured surface morphology of $NiCaF_2$ and $NiCaSO_4$ coatings after the adhesion strength test. Adhesion strength of $NiCaF_2$ and $NiCaSO_4$ coatings is observed to be 10.50 and 12 MPa respectively. From Fig. 5 it can be seen that the fracture occurred within the coating interface exhibiting cohesive failure of the coatings. This implies that the adhesion strength of the coating to the substrate is higher than the cohesive strength of the coating. Cohesive failure of coatings is due to the lower impact force of low density cenospheres and solid lubricants during spraying process. This lower impact force decreases the bonding strength within the coating constituents and leads to cohesive failure [9].

3.4. Sliding wear behavior

Fig. 6a and b demonstrates the friction coefficients of MDN 321 steel, Ni-WC, $NiCaF_2$ and $NiCaSO_4$ coatings at RT, 200, 400 and 600 °C with 20 and 40 N normal loads respectively. Tribological properties of $NiCaF_2$ and $NiCaSO_4$ coatings are compared with Ni-WC coating.MDN 321 steel and Ni-WC coating exhibited higher friction coefficient as compared to $NiCaF_2$ and $NiCaSO_4$ coatings at all the test temperatures. Friction coefficient of MDN 321 steel and all the coatings increase with increasing normal load from 20 to 40 N. At 40 N normal load friction coefficient MDN 321 steel is varies from 0.55–0.71 and displayed lower value at 600 °C and higher value at 400 °C. Formation of oxide layer at elevated temperature might be the reason for lower friction coefficient at 600 °C. Friction coefficient of Ni-WC coating at 40 N normal load varies from 0.64–0.69. It is stable at room temperature to 200 °C and exhibited lower value at 400 °C. Further, friction coefficient is higher at 600 °C owing to the oxidation of WC at higher temperature. Friction coefficient of $NiCaF_2$ and $NiCaSO_4$ coatings are similar and are lower than the MDN 321 steel and Ni-WC coating owing to lubricity property of MoS_2, CaF_2, and $CaSO_4$ across the chosen temperature range. At 40 N

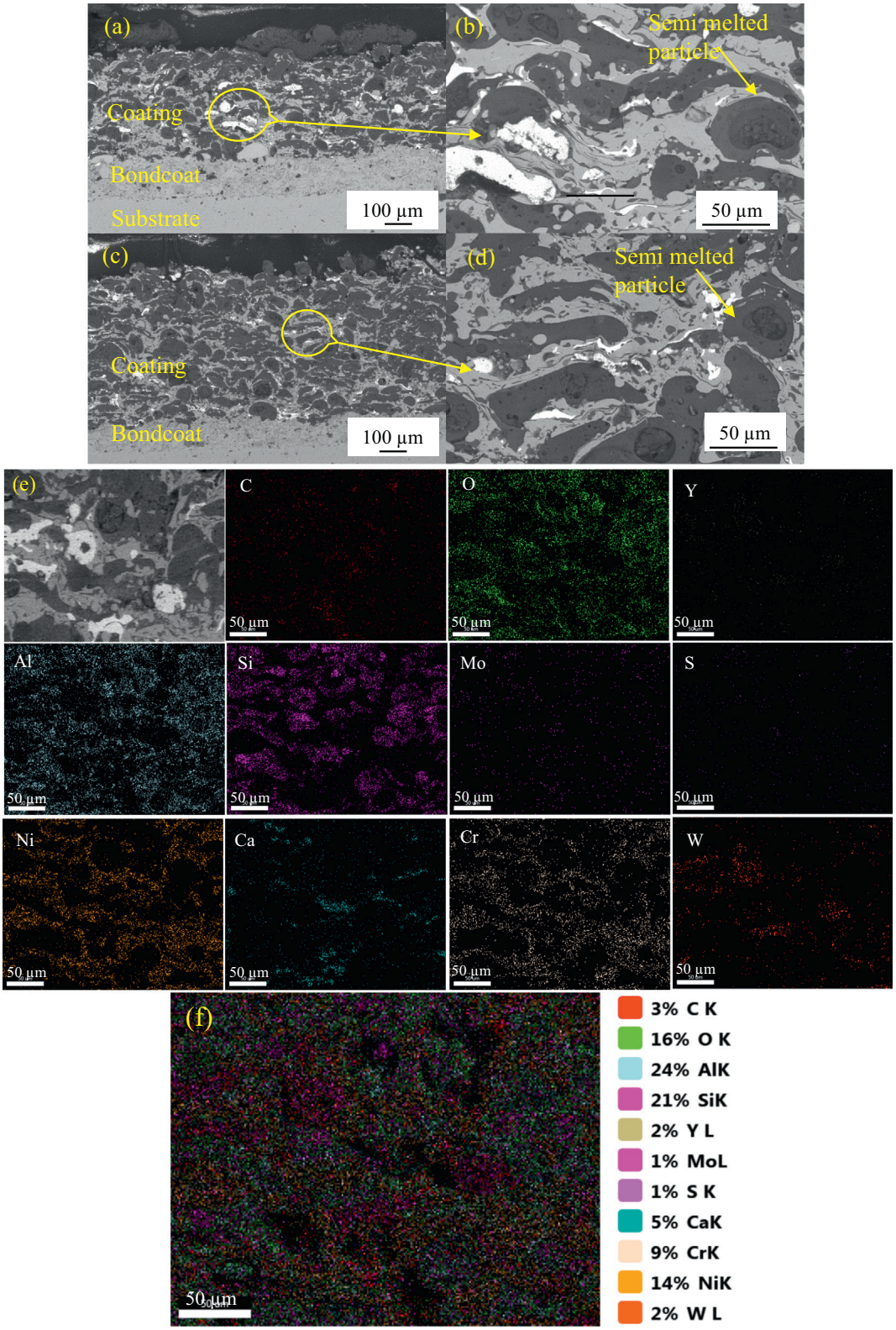

Fig. 2. Cross sectional SEM images of (a), (b) $NiCaF_2$ coating; (c), (d) $NiCaSO_4$ coating, (e) cross sectional X-ray elemental mapping of $NiCaF_2$ coating and (f) elemental overlay of the $NiCaF_2$ coating.

normal load, friction coefficient of $NiCaF_2$ and $NiCaSO_4$ coatings varies from 0.51–0.58 and 0.44–0.63 respectively. Friction coefficient of both coatings registered lower value at 600 °C and higher value at 400 °C. $NiCaF_2$ coating registered lower friction coefficient as compared to $NiCaSO_4$ coating due to lower hardness of $NiCaF_2$ coating.

Fig. 7a and b exhibits the wear rates of MDN 321 steel, Ni-WC, $NiCaF_2$ and $NiCaSO_4$ coatings at RT, 200, 400 and 600 °C with 20 and 40 N normal loads respectively. The wear rate of MDN 321 steel, Ni-WC, $NiCaF_2$ and $NiCaSO_4$ coatings increased with increasing normal load. Ni-WC, $NiCaF_2$ and $NiCaSO_4$ coatings exhibited lower wear rate as

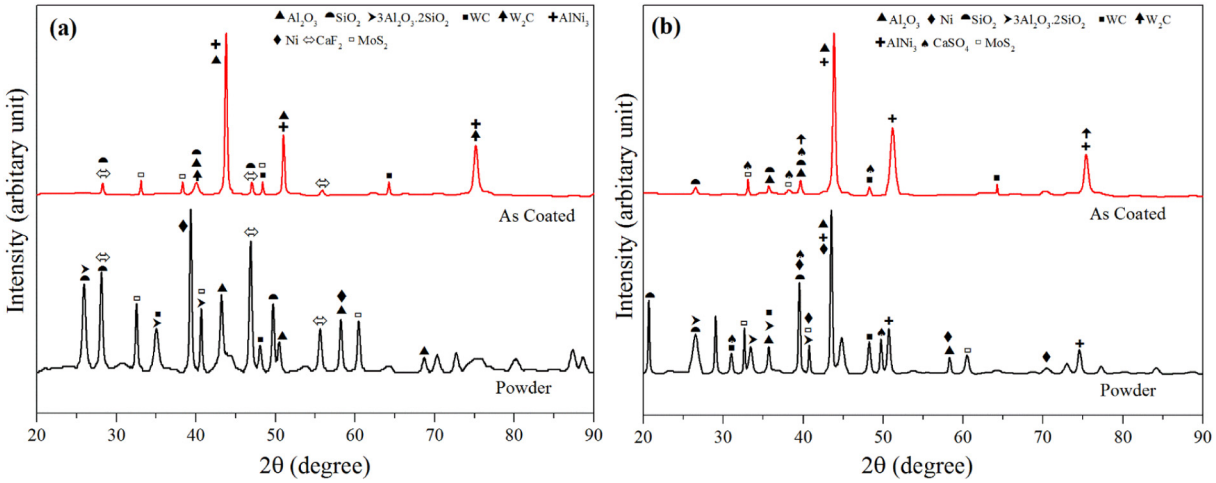

Fig. 3. XRD pattern of blended powder and as sprayed coatings of (a) $NiCaF_2$ (b) $NiCaSO_4$.

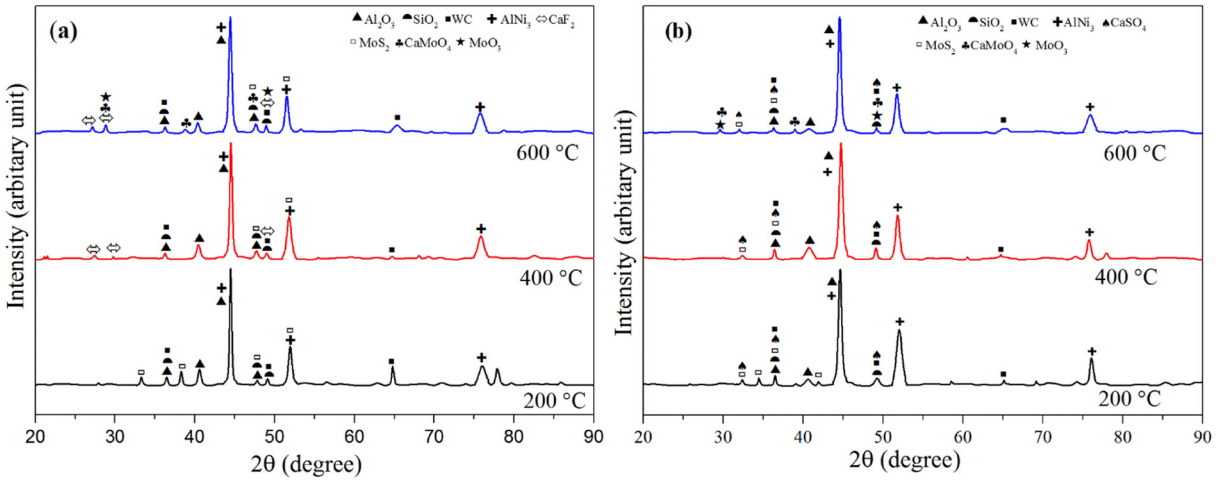

Fig. 4. XRD pattern of worn out (a) $NiCaF_2$ and (b) $NiCaSO_4$ coatings at 200, 400 and 600 °C.

compared to MDN 321 steel owing to the higher hardness of the coatings and unmelted/semi melted cenospheres in the coatings that open up amid wear test. The wear rate of MDN 321 steel is minimum at 200 °C and maximum at 400 °C under 20 and 40 N normal loads, infers rise in temperature reduces the hardness of the material leads to increasing wear rate. According to Archard's wear eq. Q = KWL/H (Q - wear volume, W - load, H - hardness of the material, K - constant and L - sliding distance), the wear rate varies inversely with the hardness. The wear rate of MDN 321 steel at 600 °C is slightly reduced owing to the formation of oxide film. Both $NiCaF_2$ and $NiCaSO_4$ coatings registered lower wear rate as compared to Ni-WC coating due to the presence of low shear strength solid lubricants in the coatings, as they form lubricating film on the rubbing surfaces. $NiCaF_2$ and $NiCaSO_4$ coatings presented marginal increase in the wear rate from RT to 200 °C. Both the coatings exhibited higher and lower wear rate at 400 and 600 °C

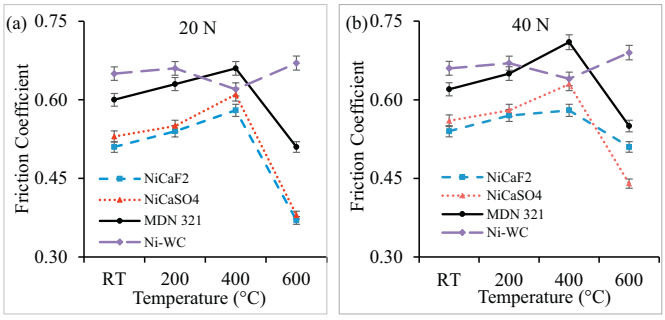

Fig. 6. Friction coefficients of MDN 321, Ni-WC, $NiCaF_2$ and $NiCaSO_4$ coatings under (a) 20 N and (b) 40 N normal loads at RT, 200, 400 and 600 °C.

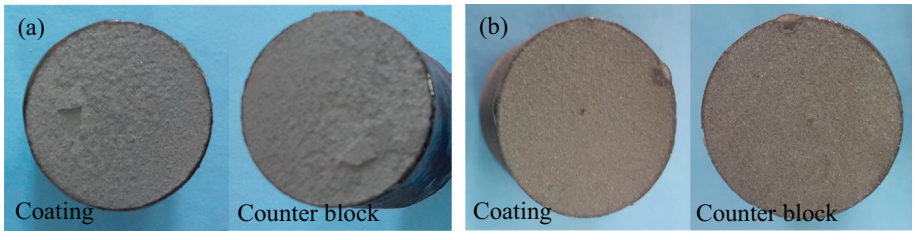

Fig. 5. Fractured surface (a) $NiCaF_2$ and (b) $NiCaSO_4$ coating after adhesion test.

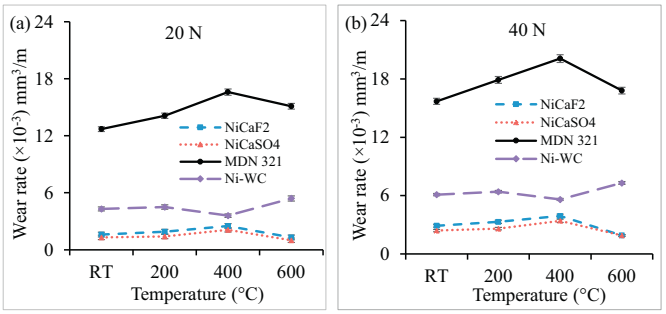

Fig. 7. Wear rates of MDN 321, Ni-WC, $NiCaF_2$ and $NiCaSO_4$ coatings under (a) 20 N and (b) 40 N normal loads at RT, 200, 400 and 600 °C.

respectively. Lower wear rate at 600 °C is attributed to the lubricating property of $CaMoO_4$, CaF_2 and $CaSO_4$ at a higher temperature. $CaMoO_4$ is formed on the sliding surface due to tribo chemistry reaction and establishes lubricating film on the surface. Following reactions shows the formation of $CaMoO_4$:

$$2MoS_2(s) + 7O_2(g) = 2MoO_3(s) + 4SO_2(g) \quad (1)$$

$$2CaF_2(s) + 2MoO_3(s) + O_2(g) = 2CaMoO_4(s) + 2F_2(g) \quad (2)$$

where, (s) and (g) represents solid and gas states respectively [40]. XRD result (Fig. 4) also confirmed the formation of $CaMoO_4$ at 600 °C. At elevated temperature, CaF_2 and $CaSO_4$ are changes from brittle to plastic behavior, thereby impart lubrication in the temperature range of 500–1000 °C. When these solid lubricants become plastic, easily spread on the sliding surface under applied load, leading to the formation lubricating film. Higher wear rate at 400 °C is due to loss of lubricating property of MoS_2 owing to its oxidization at a higher temperature and brittle form of solid lubricants (CaF_2 and $CaSO_4$) [1,40].

Figs. 8 and 9 represents the SEM images of the worn surface of $NiCaF_2$ and $NiCaSO_4$ coatings under 40 N normal load at 200, 400 and 600 °C temperatures respectively. It can be seen that the worn surfaces of both the coatings are characterized by groove, delamination and flaking pit at all the test temperatures (Figs. 8a and 9a) demonstrating plowing and delamination. From Figs. 8b and 9b, it is observed that at 400 °C worn surfaces are not smooth and coating is detached by maximum delamination suggesting severe wear. Lower wear is observed at 600 °C (Figs. 8c and 9c) characterized by smoother worn surface with minimum delamination. Figs. 8d and 9d show the worn surfaces of coatings at 200 °C with opened unmelted/semimelted cenospheres. These hollow spheres accumulate the wear debris avoiding three body abrasion leading to lower wear loss subsequently.

Fig. 10 depicts post wear test photograph of wear track and wear debris of $NiCaF_2$ coating at 200, 400 and 600 °C. From Fig. 10a it is observed that the wear track of distinct gray color is established on the disc indicating lubricating layer between the coating surface and disc. Lamella like wear debris is observed post wear test as seen in Fig. 10b–d. Wear debris seems to be much larger in size at 400 °C (Fig. 10c) as compared to 200 and 600 °C demonstrating severe wear condition at an intermediate temperature. The elemental composition of the wear debris analyzed by EDS is presented in Table 4. The elements found in wear debris are Ni, W, C, and Al which are removed from coatings. A large amount of Calcium, Fluoride, and Oxygen and small amount of Sulfur in wear debris at 400 °C implies that MoS_2 has undergone oxidation and larger amount of CaF_2 is removed. At 600 °C, the wear debris contains higher oxygen and calcium percentage indicating the formation of $CaMoO_4$ due to the chemical reaction between MoO_3 and CaF_2. $CaMoO_4$ along with CaF_2 is responsible for low friction and wear rate of coating at higher temperature.

Fig. 11 demonstrates the wear mechanism of $NiCaF_2$ coating. Fig. 11a shows the beginning stage of the wear test where coating constituents WC-Co, Cenospheres, MoS_2, and CaF_2 are distributed uniformly in the NiCrAlY matrix. Once the wear test proceeds, WC-Co, cenospheres, MoS_2 and CaF_2 emerge on the coating surface. MoS_2 and CaF_2 being soft, get extruded and spread on the worn surface of the coating. Meanwhile, all the unmelted/semimelted cenospheres in the coating open up as they are hollow and part of the debris generated as result of friction, get accumulated in broken hollow microspheres (Fig. 11b). This accumulated debris in the broken hollow spheres further acts as lubricating agent. At RT and 200 °C MoS_2 layer is formed on the coating surface leading to better lubrication (Fig. 11c). At 600 °C, high temperature solid lubricant CaF_2 gets converted from brittle to ductile providing smoothening effect thereby increasing lubrication in

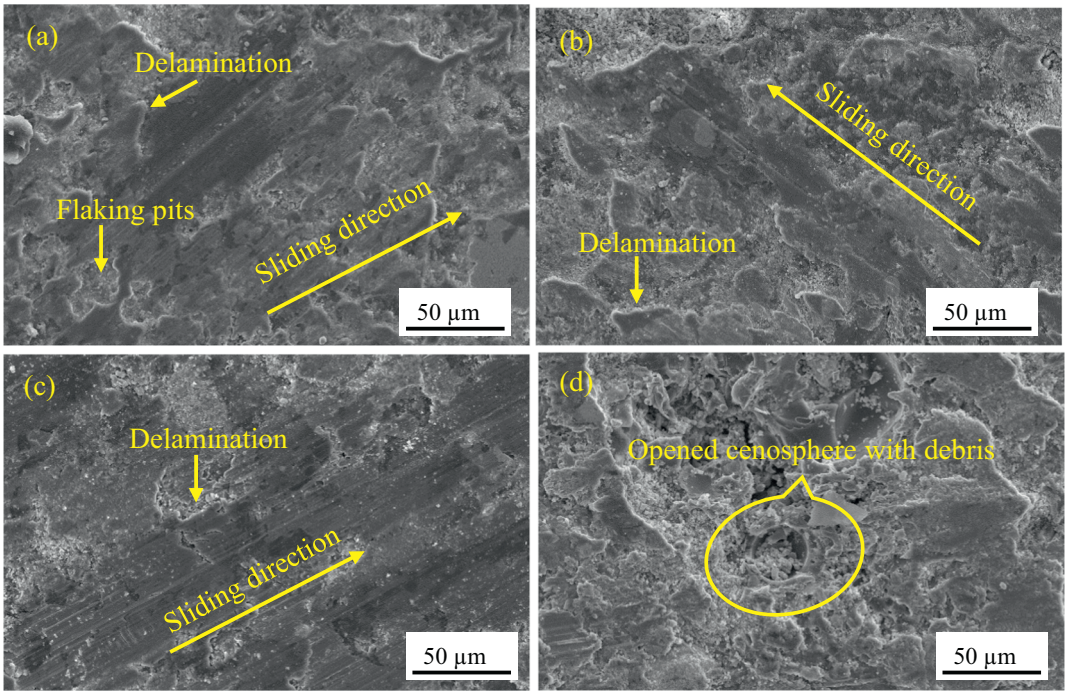

Fig. 8. SEM micrograph of worn surface of $NiCaF_2$ coating (a) 200, (b) 400, (c) 600 °C and (d) opened cenosphere with debris during wear test.

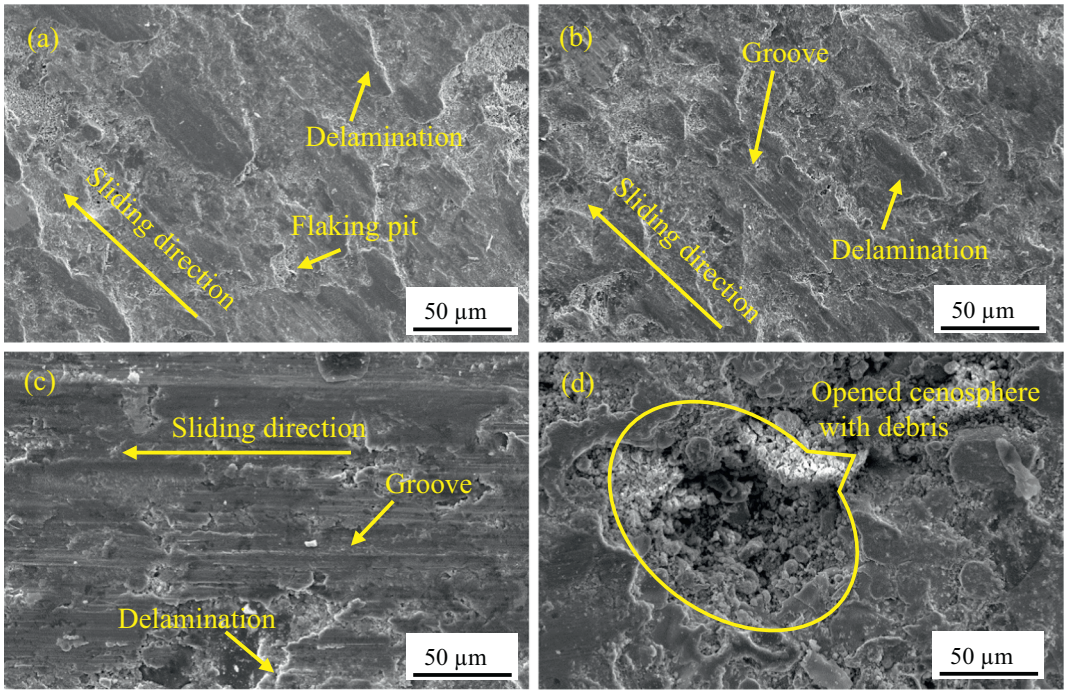

Fig. 9. SEM micrograph of worn surface of $NiCaSO_4$ coating (a) 200, (b) 400, (c) 600 °C and (d) opened cenosphere with debris during wear test.

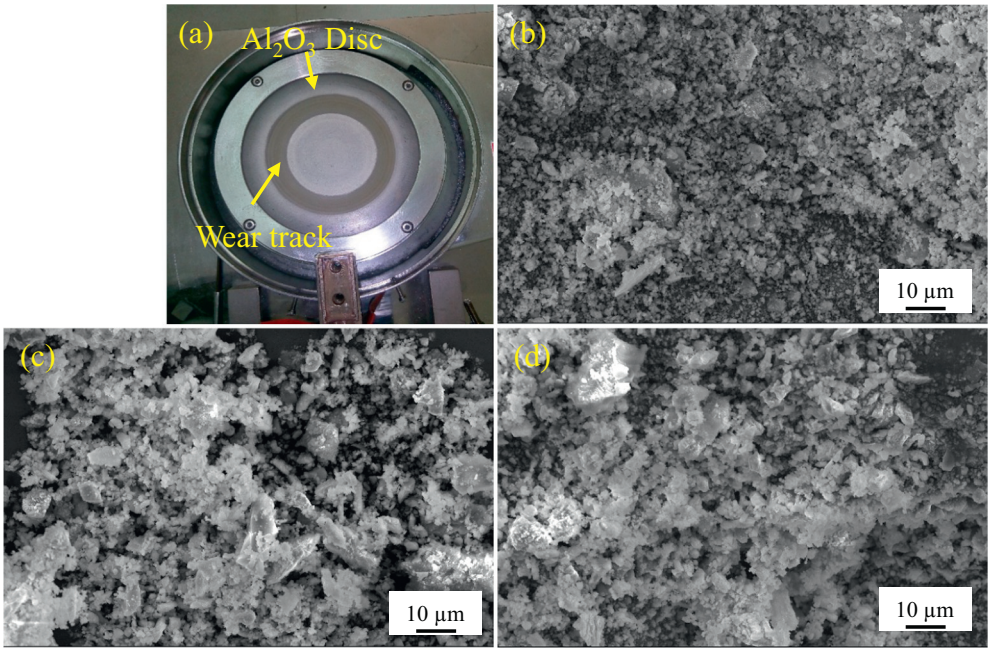

Fig. 10. Post wear test micrographs of (a) wear track of $NiCaF_2$ coating and wear debris of $NiCaF_2$ coating at (b) 200 (c) 400 and (d) 600 °C.

Table 4
EDS analysis of wear debris of $NiCaF_2$ coating at 200, 400, 600 °C.

Temperature (°C)	Elemental composition (wt%)										
	C	O	Al	Si	Ni	Cr	W	Mo	S	Ca	F
200	7.32	24.40	10.06	3.19	18.02	11.99	9.58	2.10	3.56	2.81	4.94
400	8.80	29.25	9.21	3.83	16.43	6.91	9.12	2.81	1.04	3.86	6.09
600	6.72	34.07	8.72	3.33	16.44	7.88	7.74	1.92	0.84	7.76	2.54

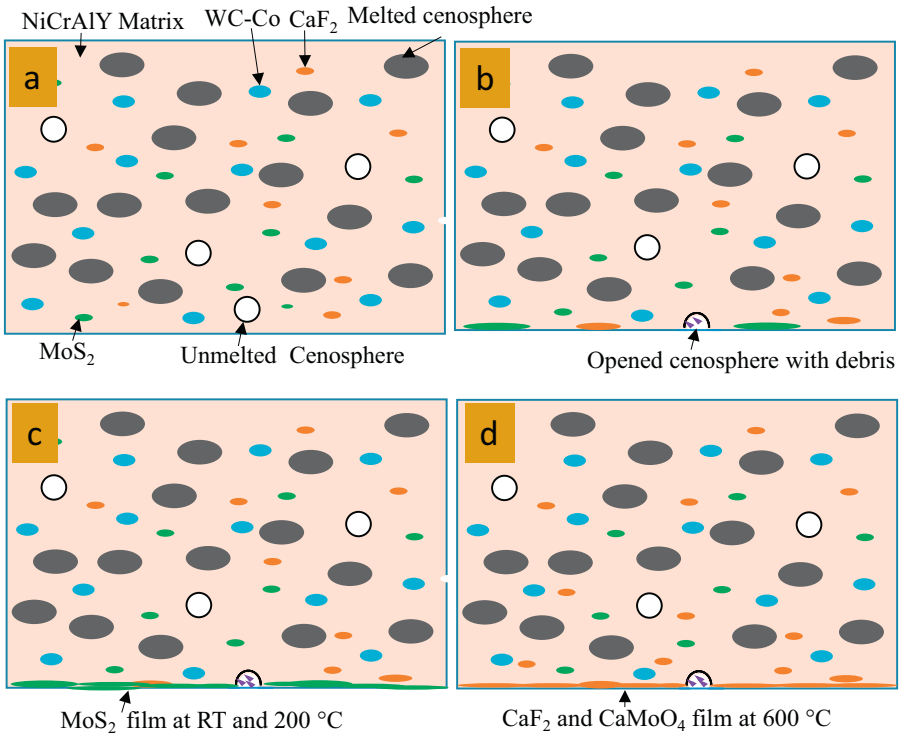

Fig. 11. Schematic diagram of the wear mechanism of $NiCaF_2$ coating at different temperatures.

the temperature range of 500–1000 °C [43]. CaF_2 become ductile and spreads over the worn surface and subsequently reacts with molybdenum oxide forming $CaMoO_4$. These CaF_2 and $CaMoO_4$ (Fig. 11d) on worn surface extends lubrication further at 600 °C. Similar trends and wear mechanism of $NiCaSO_4$ coating is observed as like in $NiCaF_2$ coating.

Both NiCaF and $NiCaSO_4$ coatings presented here are having lower friction coefficient and wear rate as compared to Ni-WC coating and MDN321steel substrate making them suitable for high temperature applications. Presence of solid lubricants and cenosphere in these coating enhances wear resistance of the coatings. Present work successfully demonstrated usage of abundantly available environmental pollutant fly ash cenospheres in the Ni-WC, $NiCaF_2$ and $NiCaSO_4$ coatings through plasma spray technique.

4. Conclusion

In the present investigation, plasma spray technique has been successfully utilized to develop $NiCaF_2$ and $NiCaSO_4$ coatings on MDN 321 steel. Tribological properties of these coatings are studied at RT, 200, 400 and 600 °C. The main conclusions can be drawn as follows:

- Ni-WC, $NiCaF_2$ and $NiCaSO_4$ coatings registered lower wear rate as compared to the MDN 321 steel substrate due to the higher hardness of the coatings and presence of unmelted/semimelted cenospheres in the coating reduces the wear loss by accumulating the wear debris in the broken hollow spheres.
- Higher wear resistance of $NiCaF_2$ and $NiCaSO_4$ coatings as compared to Ni-WC coating is attributed to the lubrication effect of solid lubricants present in the coatings.
- Friction coefficient of $NiCaF_2$ and $NiCaSO_4$ coatings is lower at 600 °C, which is at least 7.27 and 7.57% lower than the MDN 321 steel respectively.
- The wear rate of $NiCaF_2$ and $NiCaSO_4$ coatings is lower at 600 °C, which is at least 5.15 and 5.91 times lower than the MDN 321 steel respectively.
- $NiCaSO_4$ coating exhibited less wear rate at both the applied loads as compared to $NiCaF_2$ coating attributed to their higher hardness.
- $NiCaF_2$ and $NiCaSO_4$ coatings presented similar lubrication mechanism and seen to be varying with temperature. MoS_2 is the active lubricant on the sliding surface at up to 200 °C. At 400 °C, MoS_2, CaF_2, and $CaSO_4$ did not provide lubrication owing to their temperature limitations. At 600 °C, $CaMoO_4$ and MoO_3 are produced through chemical reactions, which are responsible for less friction coefficient and wear rate at elevated temperature.

Acknowledgements

The authors wish to thank Spraymet Surface Technologies Pvt. Ltd., Bangalore, India, for providing the facility of the plasma spray coating. All the authors thank Mechanical Engineering department at NITK Surathkal for providing support in carrying out this work. This research did not receive any specific grant from funding agencies in the public, commercial, or not-for-profit sectors.

References

[1] J. Chen, Y. An, J. Yang, X. Zhao, F. Yan, H. Zhou, J. Chen, Tribological properties of adaptive NiCrAlY–Ag–Mo coatings prepared by atmospheric plasma spraying, Surf. Coat. Technol. 235 (2013) 521–528.
[2] W. Wang, Application of a high temperature self-lubricating composite coating on steam turbine components, Surf. Coat. Technol. 177 (2004) 12–17.
[3] J. Zhen, J. Cheng, M. Li, S. Zhu, Z. Long, B. Yang, J. Yang, Lubricating behavior of adaptive nickel alloy matrix composites with multiple solid lubricants from 25 °C to 700 °C, Tribol. Int. 109 (2017) 174–181.
[4] H. Heshmat, P. Hryniewicz, J.F. Walton Ii, J.P. Willis, S. Jahanmir, C. Dellacorte, Low-friction wear-resistant coatings for high-temperature foil bearings, Tribol. Int. 38 (11) (2006) 1059–1075.
[5] D. Shtansky, A. Bondarev, P.V. Kiryukhantsev-Korneev, T. Rojas, V. Godinho, A. Fernández, Structure and tribological properties of MoCN-Ag coatings in the temperature range of 25–700 °C, Appl. Surf. Sci. 273 (2013) 408–414.
[6] C. Donnet, A. Erdemir, Historical developments and new trends in tribological and solid lubricant coatings, Surf. Coat. Technol. 180 (2004) 76–84.
[7] A.A. Voevodin, C. Muratore, S.M. Aouadi, Hard coatings with high temperature adaptive lubrication and contact thermal management, Surf. Coat. Technol. 257 (2014) 247–265.
[8] C. Huang, L. Du, W. Zhang, Effects of solid lubricant content on the microstructure

and properties of NiCr/Cr 3 C 2–BaF 2·CaF 2 composite coatings, J. Alloys Compd. 479 (1) (2009) 777–784.
[9] X.-F. Zhang, X.-L. Zhang, A.-H. Wang, Z.-W. Huang, Microstructure and properties of HVOF sprayed Ni-based submicron WS2/CaF2 self-lubricating composite coating, Trans. Nonferrous Metals Soc. China 19 (1) (2009) 85–92.
[10] L. Wang, B. Wang, X. Wang, W. Liu, Tribological investigation of CaF 2 nanocrystals as grease additives, Tribol. Int. 40 (7) (2007) 1179–1185.
[11] C. Baker, R. Chromik, K. Wahl, J. Hu, A. Voevodin, Preparation of chameleon coatings for space and ambient environments, Thin Solid Films 515 (17) (2007) 6737–6743.
[12] J. Chen, G. Hou, J. Chen, Y. An, H. Zhou, X. Zhao, J. Yang, Composition versus friction and wear behavior of plasma sprayed WC–(W, Cr) 2 C–Ni/Ag/BaF 2–CaF 2 self-lubricating composite coatings for use up to 600° C, Appl. Surf. Sci. 261 (2012) 584–592.
[13] G. Kim, H. Choi, C. Han, S. Uhm, C. Lee, Characterization of atmospheric plasma spray NiCr–Cr 2 O 3–Ag–CaF 2/BaF 2 coatings, Surf. Coat. Technol. 195 (1) (2005) 107–115.
[14] S. Mishra, K. Chandra, S. Prakash, Characterisation and erosion behaviour of NiCrAlY coating produced by plasma spray method on two different Ni-based superalloys, Mater. Lett. 62 (12) (2008) 1999–2002.
[15] S. Mishra, K. Chandra, S. Prakash, Erosion–corrosion performance of NiCrAlY coating produced by plasma spray process in a coal-fired thermal power plant, Surf. Coat. Technol. 216 (2013) 23–34.
[16] B. Somasundaram, R. Kadoli, M. Ramesh, Evaluation of cyclic oxidation and hot corrosion behavior of HVOF-sprayed WC-Co/NiCrAlY coating, J. Therm. Spray Technol. 23 (6) (2014) 1000–1008.
[17] H. Grewal, H. Singh, A. Agrawal, Microstructural and mechanical characterization of thermal sprayed nickel–alumina composite coatings, Surf. Coat. Technol. 216 (2013) 78–92.
[18] M. Jafari, M. Enayati, M. Salehi, S. Nahvi, C. Park, Microstructural and mechanical characterizations of a novel HVOF-sprayed WC-Co coating deposited from electroless Ni–P coated WC-12Co powders, Mater. Sci. Eng. A 578 (2013) 46–53.
[19] J. Voyer, B.R. Marple, Tribological performance of thermally sprayed cermet coatings containing solid lubricants, Surf. Coat. Technol. 127 (2) (2000) 155–166.
[20] C. Bin, Y.-F. Tan, H. Long, T. Hua, X.-L. Wang, Tribological behavior and mechanisms of graphite/CaF2/TiC/Ni-base alloy composite coatings, Trans. Nonferrous Metals Soc. China 23 (2) (2013) 392–399.
[21] V. Manakari, G. Parande, M. Doddamani, V. Gaitonde, I. Siddhalingeshwar, V.C. Shunmugasamy, N. Gupta, Dry sliding wear of epoxy/cenosphere syntactic foams, Tribol. Int. 92 (2015) 425–438.
[22] B.R. Bharath Kumar, M. Doddamani, S.E. Zeltmann, N. Gupta, M.R. Ramesh, S. Ramakrishna, Processing of cenosphere/HDPE syntactic foams using an industrial scale polymer injection molding machine, Mater. Des. 92 (2016) 414–423.
[23] S.E. Zeltmann, B.R. Bharath Kumar, M. Doddamani, N. Gupta, Prediction of strain rate sensitivity of high density polyethylene using integral transform of dynamic mechanical analysis data, Polymer 101 (2016) 1–6.
[24] B.R. Bharath Kumar, M. Doddamani, S.E. Zeltmann, N. Gupta, Uzma, S. Gurupadu, R.R.N. Sailaja, Effect of particle surface treatment and blending method on flexural properties of injection-molded cenosphere/HDPE syntactic foams, J. Mater. Sci. 51 (8) (2016) 3793–3805.
[25] D. M.R., K. S.M., Kishore, Behavior of sandwich beams with functionally graded rubber core in three point bending, Polym. Compos. 32 (10) (2011) 1541–1551.
[26] M. Doddamani, S.M. Kulkarni, Dynamic response of fly ash reinforced functionally graded rubber composite sandwiches-a Taguchi approach, Int. J. Eng. Sci. Technol. 3 (1) (2011) 17.
[27] B.B. Kumar, A.K. Singh, M. Doddamani, D.D. Luong, N. Gupta, Quasi-static and high strain rate compressive response of injection-molded cenosphere/HDPE syntactic foam, JOM 68 (7) (2016) 1861–1871.
[28] B.B. Kumar, M. Doddamani, S.E. Zeltmann, N. Gupta, S. Ramakrishna, Data characterizing tensile behavior of cenosphere/HDPE syntactic foam, Data Brief 6 (2016) 933–941.
[29] M. Doddamani, V.C. Shunmugasamy, N. Gupta, H. Vijayakumar, Compressive and flexural properties of functionally graded fly ash cenosphere–epoxy resin syntactic foams, Polym. Compos. 36 (4) (2015) 685–693.
[30] B.R. Bharath Kumar, S.E. Zeltmann, M. Doddamani, N. Gupta, Uzma, S. Gurupadu, R.R.N. Sailaja, Effect of cenosphere surface treatment and blending method on the tensile properties of thermoplastic matrix syntactic foams, J. Appl. Polym. Sci. 133 (35) (2016) (p. n/a-n/a).
[31] M.L. Jayavardhan, B.R. Bharath Kumar, M. Doddamani, A.K. Singh, S.E. Zeltmann, N. Gupta, Development of glass microballoon/HDPE syntactic foams by compression molding, Compos. Part B 130 (2017) 119–131.
[32] A. Arizmendi-Morquecho, A. Chávez-Valdez, J. Alvarez-Quintana, High temperature thermal barrier coatings from recycled fly ash cenospheres, Appl. Therm. Eng. 48 (2012) 117–121.
[33] S. Das, S. Ghosh, A. Pandit, T. Bandyopadhyay, A. Chattopadhyay, K. Das, Processing and characterisation of plasma sprayed zirconia–alumina–mullite composite coating on a mild-steel substrate, J. Mater. Sci. 40 (18) (2005) 5087–5089.
[34] S. Mishra, K. Rout, P. Padmanabhan, B. Mills, Plasma spray coating of fly ash premixed with aluminium powder deposited on metal substrates, J. Mater. Process. Technol. 102 (1) (2000) 9–13.
[35] M. Muhammad, A. Jalar, R. Shamsudin, M. Isa, Effect of plasma spray parameters on porosity of fly ash deposited coatings, AIP Conference Proceedings, AIP, 2014.
[36] L.R. Krishna, D. Sen, D.S. Rao, G. Sundararajan, Coatability and characterization of fly ash deposited on mild steel by detonation spraying, J. Therm. Spray Technol. 12 (1) (2003) 77–79.
[37] B.S. Sidhu, H. Singh, D. Puri, S. Prakash, Wear and oxidation behaviour of shrouded plasma sprayed fly ash coatings, Tribol. Int. 40 (5) (2007) 800–808.
[38] A. Behera, S. Mishra, Application of Fly-ash Composite in Plasma Surface Engineering, (2012).
[39] B. Li, J. Jia, Y. Gao, M. Han, W. Wang, Microstructural and tribological characterization of NiAl matrix self-lubricating composite coatings by atmospheric plasma spraying, Tribol. Int. 109 (2017) 563–570.
[40] L. Kong, Q. Bi, M. Niu, S. Zhu, J. Yang, W. Liu, ZrO 2 (Y 2 O 3)–MoS 2–CaF 2 self-lubricating composite coupled with different ceramics from 20 °C to 1000 °C, Tribol. Int. 64 (2013) 53–62.
[41] M. Mathapati, M. Ramesh, M. Doddamani, High temperature erosion behavior of plasma sprayed NiCrAlY/WC-Co/cenosphere coating, Surf. Coat. Technol. 325 (2017) 98–106.
[42] J. Chen, X. Zhao, H. Zhou, J. Chen, Y. An, F. Yan, Microstructure and tribological property of HVOF-sprayed adaptive NiMoAl–Cr 3 C 2–Ag composite coating from 20 °C to 800 °C, Surf. Coat. Technol. 258 (2014) 1183–1190.
[43] I. Allam, Solid lubricants for applications at elevated temperatures, J. Mater. Sci. 26 (15) (1991) 3977–3984.